Three dimensional structures of the geometrically necessary dislocations in matrix-inclusion systems under uniaxial tensile loading

Tetsuya Ohashi *
Kitami Institute of Technology, Koencho 165, Kitami, Hokkaido, Japan

Abstract
Plastic slip deformation in matrix-inclusion systems, in which a cuboidal or spherical shaped inclusion is embedded in a softer matrix, are numerically analyzed by a finite element technique. Edge and screw components of the geometrically necessary dislocations on slip systems are evaluated for each finite element from the spatial gradient of plastic shear strain. The character of the dislocation segments in each element is deduced from the data for edge and screw components and the directions of dislocation segments are determined. The aggregate of the dislocation segments in the whole specimen shows typical structures of dislocations, such as the Orowan loops around the inclusion and tilt boundaries that develop perpendicular to the primary slip plane. Stress state and shape of dislocations in deformable inclusions are discussed.

Keywords: A, dislocations; A, microstructures; A, voids and inclusions; B, crystal plasticity; Orowan loops.

* e-mail ohashi@newton.mech.kitami-it.ac.jp, tel./fax. +81-157-26-9227

1. Introduction

Alloying of metallic materials sometimes ends with a generation of precipitates or inclusions in the microstructure. The mechanical behavior of the inclusions is usually different from that of the matrix and the interaction of dislocations with the inclusions changes not only with their mechanical characters but also with their geometrical shape, their spatial arrangement, amount and character of the strain field which is formed as a result of precipitation process, and so on. It is well known that the movement of dislocations in the matrix-inclusion system results in the formation of Orowan loops of dislocations when large inclusions are sparsely distributed and the resistance to the movement of dislocations in the inclusion is larger than that in the matrix. Accumulation of the Orowan type dislocations has significant effects on the macroscopic characteristics of yielding, strain hardening, or creep behavior and at the same time, they will contribute to the generation of voids and prismatic dislocation loops (Hirsch, 1975) or nucleation of recrystallization (Humphreys, 2000) at the phase boundary between the matrix and inclusion. Therefore, the microscopic aspects of slip processes in the matrix-inclusion system are important not only for the prediction of their macroscopic mechanical response but also from the view point of the design of materials.

Plastic deformation in a microstructure with inclusions has been studied theoretically, experimentally and numerically. Hart (1972) introduced a dislocation concept for the prediction of macroscopic strain hardening in dispersion hardened alloys. Nagayama *et al.* (1986) used finite element

axisymmetric models where a single inclusion was embedded in the matrix and they discussed plastic strain fields in the microstructure. Ishikawa *et al.* (2000) showed a numerical approach for the analysis of deformation in a microstructure with a periodic particle array of hard phase in Ferrite-Pearlite steels and discussed the microscopic deformation fields and the macroscopic response of the whole specimen. Busso *et al.* (2000) and Fedelich (2002) estimated the macroscopic mechanical response of nickel-base superalloys on the basis of models for the movement and accumulation of dislocations in the γ–γ' microstructures. McHugh *et al.* (1991, 1993) and Bruzzi *et al.* (2001) numerically explored plastic slip deformation in Al-Cu/SiC microstructure by crystal plasticity analysis and discussed the relation between the volume fraction of the second particles and the macroscopic flow stress level. Macroscopic mechanical response and yield surfaces of matrix-inclusion systems as well as internal stresses generated in the microstructure by the presence of second phase particles were also analyzed numerically on the basis of self-consistent approach [for example, Bonfoh *et al*. (2003a), Bonfoh *et al*. (2003b), and Schmitt *et al*. (1997)]. Growth and coalescence of microvoids in microstructures were also modeled and analyzed numerically [for example, Schacht *et al.* (2003), Li and Guo (2003), and Li *et al.* (2003)]. On the other hand, details of the structure of dislocations around second particles has been investigated theoretically and experimentally (Hirsch, 1975), and recently, elaborate studies on the equilibrium position of circular dislocation loops at a short rigid fiber (Khraishi and Zbib, 2002) and on the thermally activated passage of dislocations through obstacles (Hiratani *et al.*, 2003) were made by dislocation dynamics simulation, while the relation between the dislocation

accumulation and non-uniform deformation fields in the matrix-inclusion system is not yet fully understood. In the present paper, we employ a two phase material model in which a single inclusion is embedded in a f.c.c. matrix, and analyze slip deformation of the model under uniaxial load using a three dimensional crystal plasticity simulation code (Ohashi, 1987, 1994). The density distribution of the geometrically necessary dislocations is evaluated from gradients of plastic shear strains on twelve slip systems and three dimensional images for the dislocation structure are obtained.

2. Basic equations for the crystal plasticity analysis

Let us consider slip deformation in face centered cubic type crystals, where slip takes place on the {111} crystal planes and in the <110> crystal directions. The combinations of these slip planes and these slip directions define twelve slip systems. Table 1 shows the definition of the twelve slip systems used in this paper. The activation condition of the slip system n is assumed to be given by the Schmid law:

$$P_{ij}^{(n)}\sigma_{ij} = \theta^{(n)}, \quad P_{ij}^{(n)}\dot{\sigma}_{ij} = \dot{\theta}^{(n)}, \quad (n = 1,\cdots,12), \tag{1}$$

and,

$$P_{ij}^{(n)} = \frac{1}{2}\left(\nu_i^{(n)}b_j^{(n)} + \nu_j^{(n)}b_i^{(n)}\right), \tag{2}$$

where, σ_{ij} and $\theta^{(n)}$ denote the stress and the critical resolved shear stress on slip system n, respectively. The Schmid tensor $P_{ij}^{(n)}$ is defined by the slip plane normal $\nu_i^{(n)}$ and the slip direction $b_i^{(n)}$. Quantities with dots indicate incremental quantities. An increment of the critical resolved shear stress is written as follows:

$$\dot{\theta}^{(n)} = \sum_m h^{(nm)}\dot{\gamma}^{(m)}. \tag{3}$$

Here, $\dot{\gamma}^{(m)}$ denotes the increment of the plastic shear strain on slip system m. If the deformation is small and rotation of the crystal orientation is neglected, the constitutive equation for slip deformation is written as follows (Hill, 1966; Ohashi, 1987):

$$\dot{\varepsilon}_{ij} = [S^{e}_{ijkl} + \sum_{n}\sum_{m}\{h^{(nm)}\}^{-1}P^{(n)}_{ij}P^{(m)}_{kl}]\dot{\sigma}_{kl}\,. \tag{4}$$

S^{e}_{ijkl} denotes the elastic compliance, and the summation is made over the active slip systems.

Let us suppose that the critical resolved shear stress is a function of the Bailey-Hirsch type and given by the following equation (Ohashi, 1987, 1994):

$$\theta^{(n)} = \theta_0 + \sum_{m}\Omega^{(nm)}a\mu\tilde{b}\sqrt{\rho^{(m)}_{a}}\,, \tag{5}$$

where, θ_0 and $\rho^{(m)}_{a}$ denote the lattice friction term, which is temperature-dependent in general, and the dislocation density that accumulates on slip system m, respectively. In this paper, we assume that the temperature is a constant, and then, θ_0 is also a constant. The interaction of slip systems n and m is controlled by the interaction matrix $\Omega^{(nm)}$. There are 12 x 12 components in $\Omega^{(nm)}$ and their values are given by five independent parameters which are defined by elementary processes of interaction between dislocations on slip systems n and m (Ohashi, 1987, 1994). Table 2 shows the dislocation interaction and components of the interaction matrix, R1, R2, R3,

R3', and R4. The relative magnitude of the off diagonal to the diagonal components in the interaction matrix governs the latent hardening characteristics of slip systems. In the present study, we choose parameters as $\mathrm{R1} \approx \mathrm{R2} \approx \mathrm{R3} \approx \mathrm{R3}' \approx \mathrm{R4} \approx 1$ to represent a nearly isotropic hardening character for every slip system. The elastic shear modulus μ and the magnitude of the Burgers vector $\tilde{b}$ are supposed to be material constants and a is a numerical factor on the order of 0.1.

The dislocation density on slip system n is given by the following equation:

$$\rho_a^{(n)} = s\rho_S^{(n)} + g\left\|\rho_G^{(n)}\right\|, \tag{6}$$

where, $\rho_S^{(n)}$ and $\left\|\rho_G^{(n)}\right\|$ denote the densities of the statistically stored and the geometrically necessary dislocations, and numerical parameters s and g are introduced to control the complexity of the simulation. It is still a point of controversy (Weertman, 2002) whether the geometrically necessary dislocations contribute directly to the strain hardening. In the present paper, we define s=1 and g=0 for simplicity (see the second footnote in section 3).

The increment in the density of the statistically stored dislocations on the slip system n is given as follows (Ohashi, 1987, 1994):

$$\dot{\rho}_S^{(n)} = {c\dot{\gamma}^{(n)}}\Big/{\tilde{b}L^{(n)}}, \tag{7}$$

where, $L^{(n)}$ is the mean free path of dislocations on slip system n, and c is a

numerical coefficient on the order of 1. Some of the possible models for the mean free path and their effect on macroscopic mechanical response are discussed elsewhere (Ohashi, 1994). The density of the geometrically necessary dislocations is given by (Ohashi, 1999):

$$\left\|\rho_G^{(n)}\right\| = \sqrt{\left(\rho_{G,edge}^{(n)}\right)^2 + \left(\rho_{G,screw}^{(n)}\right)^2}, \tag{8}$$

and the edge and screw components are defined by the strain gradients:

$$\rho_{G,edge}^{(n)} = -\frac{1}{\tilde{b}}\frac{\partial\gamma^{(n)}}{\partial\xi}, \qquad \rho_{G,screw}^{(n)} = \frac{1}{\tilde{b}}\frac{\partial\gamma^{(n)}}{\partial\zeta}. \tag{9}$$

Here, ξ and ζ denote, respectively, directions parallel and perpendicular to the slip direction on the slip plane. Evaluation of the edge and screw components for the geometrically necessary dislocations enables one to calculate the tangent vector $\mathbf{l}^{(n)}$ of the dislocation line segments as follows:

$$\mathbf{l}^{(n)} = \frac{1}{\left\|\rho_G^{(n)}\right\|}\left(\rho_{G,screw}^{(n)} \cdot \mathbf{b}^{(n)} + \rho_{G,edge}^{(n)} \cdot \mathbf{b}^{(n)} \times \mathbf{v}^{(n)}\right), \tag{10}$$

where, $\mathbf{b}^{(n)}$ and $\mathbf{v}^{(n)}$ are unit vectors parallel to the slip direction of the slip system n, and perpendicular to the slip plane, respectively. The angle φ between a dislocation line segment and the Burgers vector defines the character of the segment. It is given by:

$$\cos\varphi^{(n)} = \frac{\rho_{G,screw}^{(n)}}{\left\|\rho_G^{(n)}\right\|}, \qquad \sin\varphi^{(n)} = \frac{\rho_{G,edge}^{(n)}}{\left\|\rho_G^{(n)}\right\|}. \tag{11}$$

Positive and negative edge dislocation segments have the characteristic angles $\pi/2$ and $3\pi/2$, respectively, while negative and positive screws dislocation segments have the characteristic angles 0 and π. Numerical results for the edge and screw components are, in general, finite and "pure" edge or screw segments will never be obtained. The terms "edge" or "screw" segments used in the following description always bear the meaning of "approximately pure" edge or screw segments.

From eqs. (3), (5)-(7), and using s=1 and g=0, the hardening coefficient $h^{(nm)}$ is obtained as follows:

$$h^{(nm)} = \frac{ac\mu\Omega^{(nm)}}{2L^{(m)}\sqrt{\rho_S^{(m)}}}. \tag{12}$$

3. Model microstructures employed for the analysis

Figure 1 shows the model microstructure of two phase material employed in the present paper where an inclusion of cuboidal or spherical shape is embedded in the center of the matrix. The lateral dimension of the cuboidal inclusion and the diameter of the spherical one is 4 μm, while the lateral dimension of the whole specimen is 30 μm. The crystal orientation is shown in Figure 2. The models are subjected to a uniaxial tensile load in the y direction. The slip direction [101] and the slip plane normal $(11\bar{1})$ of the primary slip system under the tensile load lie parallel to the x-y plane and the Schmid factor for the slip system is 0.5. The arrangement of the slip plane and slip direction of the primary slip system is shown also in Figure 1. The effect of lattice misfit between the inclusion and the matrix is not considered in this paper.

The elastic compliances for the inclusion and matrix are given the same values, which are S_{11}=1, S_{12}=-0.25, and S_{44}=2.5 $\times 10^{-11}$ [m^2/Pa], and their elastic anisotropy ratio A=1[†]. The lattice friction for the matrix θ_0 is taken as 50 MPa. We employ two types of material properties for inclusions; one is a non-deformable type and the other is a deformable one. The lattice friction

[†] We also examined the structure of GN dislocations when the elastic compliances for the inclusion are 20% less than the values given here. The dislocations at the earliest stage of plastic slip were observed to accumulate near the top and bottom of the inclusion due to the elastic stress concentration. As the plastic slip deformation proceeded, the effect of non-uniform distribution of elastic stresses faded away, and the dislocation structures developed into a similar one described in the section 4.1.

stresses for the non-deformable and deformable inclusions are 1 GPa and 75 MPa, respectively. The slip deformation will then take place only in the matrix in the model with non-deformable inclusions and the inclusions will deform only elastically. In the models with deformable inclusions, the slip takes place in the matrix first, and then it will penetrate into the inclusion. With these conditions, the accumulation of dislocations takes place due to the difference of lattice frictions for the two phases.

The magnitude of the Burgers vector $\tilde{b}$ is a typical value of 2.5×10^{-10} m. The mean free path $L^{(n)}$ is given a sufficiently large value of 10^{-3} m in the present paper. As a result, the increase in the density of statistically stored dislocations is almost zero and the strain hardening is negligibly small[‡].

The densities of the edge and screw components of the GN dislocations are calculated at the center of each finite element. Once we obtain density components for the geometrically necessary dislocations in each element, we can draw dislocation line segment(s) in the elements.

In the graphical representation, we define the length and thickness of the dislocation segments as a function of the density norm $\left\|\rho_G^{(n)}\right\|$ and for the sake of simplicity and clarity of graphics, we introduce a "filter" as shown in Figure 3. Dislocation segments with density smaller than d_1 are not displayed in the graphics and the length of the dislocation segments at sites where $d_1 < \left\|\rho_G^{(n)}\right\| < d_2$ increases with density and their thickness are the same, while the

[‡] The effect of strain hardening on the structure of GN dislocations, and vice versa, is another point of interest and it will be discussed elsewhere (Ohashi, 2003).

dislocation segments with $d_2 < \left\| \rho_G^{(n)} \right\| < d_3$ are given the same length but their thicknesses increase with the density. Dislocation segments at sites where their density is larger than d_3 are displayed by line segments with the same length and thickness. We can also assign dislocation segments a color, which is determined as a function of their characteristic angle (Ohashi, 1999). If we observe a clockwise loop of dislocation segments, within which plastic shear strain is larger than that outside the loop, its graphical representation should be something like the one given in Figure 4.

The whole specimen was divided into finite element in a various way, first, to check adequacy of the meshing. The minimum and the maximum of the number of elements tested are 2744 and 27000, and we find that the results of analyses are essentially the same when the number is larger than 8000. Thus the whole specimen is divided into 8000 finite elements in the following analyses. Mesh size is finer near the phase boundary, especially in the direction perpendicular to it. The element type used in this study is a composite element with eight nodes (Zienkiewicz, 1977). One composite element consists of five tetrahedral elements with linear shape functions. The deformation behavior is analyzed with the tetrahedral elements, while the data for dislocations are evaluated for each composite element with averaged data for stresses and strains in the tetrahedral elements. Nodal point data of the plastic shear strain on twelve slip systems are evaluated by weighted average of the values in composite elements which are connected to the node, and the strain gradients in elements are calculated from the nodal point data (Ohashi, 1997). For the time marching of the incremental analysis, we extend the

algorithm proposed by Yamada, *et al.* (1968). In this extended algorithm, small and varying increments of load sufficient to just cause activation of the successive slip systems or inactivation of an active system are applied. The constitutive relation of the element is revised in accordance with the new set of active slip systems and a new time step is then started.

4. Results and discussion

4.1 Wall and loop shaped structure of GN dislocations

Figure 5(a) shows the structure of GN dislocations on the primary slip system around the cuboidal shaped inclusion. The whole specimen is deformed until the average tensile strain is 0.51%. Dislocation densities just near the matrix-inclusion interface are about 2-3 x 10^{12} m^{-2}. There are loop shaped structures of GN dislocations, which are formed close to the interface as illustrated by L1 in Figure 5(b). Dislocation line segments with the L1 structure make up single directional loops and they correspond to the Orowan loops. The suppression of plastic shear strain near the interface results in the formation of this type of structure. Another type of dislocation structure is also observed in Figure 5(a); two dislocation walls grow in the direction perpendicular to the slip plane. These walls, illustrated and denoted as W1 and W2 in Figure 5(b), consist of negative (φ=3π/2) and positive (φ=π/2) edge dislocation segments, respectively. Walls of edge dislocations with the same sign rotate crystal orientation and this structure is usually called tilt boundary (Humphreys and Hatherly, 1996). A pair of dislocation walls with positive and negative sign will cause double orientation change, and the structure with this type of dislocation walls is usually called a kink band (Humphreys and Hatherly, 1996).

The structure of GN dislocations generated near a spherical inclusion is more complicated. Figure 6 shows the structure when the specimen is deformed until the average tensile strain is 0.27 %. The average plastic shear

strain on the primary slip system is about 0.33% and the maximum and minimum values are about 0.48 and 0.13% in the matrix region. We again observe tilt boundaries that grow perpendicular to the slip plane, and they consist of negative and positive edge dislocation segments. Between these tilt boundaries, dislocation segments with screw and mixed characters exist. We also observe arch shaped structures next to the tilt boundaries and small loops are seen on the top of the inclusion. Let us examine these structures in detail.

To examine the structure of GN dislocations at the spherical shaped inclusion, we cut out thin foils from the specimen. The foils are parallel to the primary slip plane and positioned as illustrated in Figure 7. The thickness of the foils f1 and f2 is the same and is 1.0 μm and they are positioned at the offsets of 1.7 and 3.5 μm from the center of the inclusion, respectively. The foil f3 penetrates the inclusion at its center and its thickness is 0.2 μm. Figure 8 shows the structure of GN dislocations observed in the foils f1-f3. In the foil f1, we observe small clockwise dislocation loops and U shaped structures (Figure 8(a) and (b)). Dislocation segments at the bottom of the U shaped structures also contribute to the loop structure. In the foil f2, counterclockwise loops and small clockwise ones are seen (Figure 8(c) and (d)). The counterclockwise loops are formed around the inclusion and these correspond to the Orowan loops. Smaller clockwise loops emerge from the inclusion-matrix interface. In the foil f3, the dislocation structure is similar to that in the foil f2, except that large counterclockwise loops are not complete (Figure 8(e) and (f)).

Loop shaped structures of GN dislocations are, in general, formed along the boundary of a region where plastic shear strain differs from its environment.

The sense of the loop depends on the relative magnitude of the shear strain inside and outside of the region; clockwise loops are formed around a region where the strain is larger, while, regions with relatively small plastic shear strain are bounded by counterclockwise loops. Small clockwise loops, as we observe in the foils f1-f3, indicate that there are increased shear strain distributions near the inclusion-matrix interface, while larger structures of counterclockwise loops show suppression of plastic shear. Non-uniform stress fields in the vicinity of the phase boundary, which are generated after plastic slip, are thought to be responsible for this complex nature of dislocation structure (Ohashi and Asakawa, 2002).

Figure 9 shows the maximum densities of GN dislocations observed in the twelve slip systems. The primary slip system is denoted by b4. Several secondary slip systems are active and the a3 slip system is prominent among them. Figure 10 shows the distribution of GN dislocations on the a3 slip system. The distribution of dislocations is confined near the phase boundary and the whole structure is made up of four cone-shaped aggregates of GN dislocations and each cone consists of small dislocation loops.

4.2 GN dislocations in microstructures with deformable inclusions

Figure 11(a) and (b) show the structures of GN dislocations on the primary (b4) slip system in microstructures with deformable inclusions. In the microstructure with the cuboidal shaped inclusion, dislocations enter into the inclusion keeping a rather straight shape and shrink into a small ellipse to annihilate at the center. Dislocations in the spherical shaped inclusion do not

show a straight form but curve to form dislocation half loops. These half loops within the inclusion seem to connect to the half loops outside the inclusion. Dislocation density in the cuboidal shaped inclusion is comparable to that outside the inclusion, while the density in the spherical shaped one is very small. Figure 12(a) and (b) compare the density distribution of the norm $\left\|\rho_G^{(b4)}\right\|$ in the microstructure with cuboidal and spherical shaped inclusions. The double wall structure of dislocations penetrates the cuboidal shaped inclusion and the maximum density exists within it. The dislocation structure at the spherical shaped inclusion grows in a more isotropic manner, compared to that at the cuboidal shaped one, and the dislocation density in the inclusion is much smaller than that outside the inclusion. This result reflects the difference in the distribution of stress and strain in the interior of the inclusions; the stress and the plastic slip strain is approximately uniform in the spherical one, while there remains a distinct non-uniform distribution of stress, and thus slip strain, in the cuboidal inclusion even though the stress distribution is flattened after plastic slip in the inclusion.

Table 3 compares the stress state in the deformable and non-deformable inclusion with cuboidal shape. The stress is a tension-compression bi-axial state in both cases and stress component magnitudes are reduced due to plastic slip. It should be noted that σ_{yy} multiplied by the Schmid factor (=0.5) is smaller than the critical resolved shear stress (75MPa) for the deformable inclusion. Therefore, the onset of plastic slip in the interior of the deformable inclusion is aided by the multi-axial stress state, which is formed by preceding plastic slip in the softer matrix area.

5. Summary

Plastic slip deformation in matrix-inclusion systems, in which a cuboidal or spherical shaped inclusion was embedded in a softer matrix, was numerically studied by crystal plasticity analysis and the structure of the geometrically necessary dislocations on the primary and a secondary slip systems was examined. The results are summarized as follows;

(1) Orowan type dislocation loops were formed around inclusions due to suppression of plastic slip by the inclusions. Dislocation walls, which were made up of positive or negative dislocation segments, were also observed to grow in the direction perpendicular to the primary slip plane.

(2) Small and clockwise dislocation loops and U-shaped dislocation structures were also formed around the spherical shaped inclusion.

(3) Dislocations on the secondary slip systems were confined near the matrix-inclusion interface and they formed small cone-shaped structures.

(4) When the inclusion was plastically deformable, the density and shape of the dislocations was shown to depend strongly on the shape of inclusions.

Acknowledgements

This work was done under a financial support from the project of "Research and development for applying advanced computational science and technology (ACT-JST)" at Japan Science and Technology Corporation (JST). Mr. Kazuhisa Asakawa is also acknowledged for his elaboration on geometrical modeling and numerical work during his thesis work at Kitami Institute of Technology.

REFERENCE

Bonfoh, N., Carmasol, A., and Lipinski, P., 2003. Modeling of intra-crystalline hardening of materials with particles. Int. J. Plast. 19, 1167-1193.

Bonfoh, N., Lipinski, P., Carmasol, A, and Tiem, S., 2003. Micromechanical modeling of ductile damage of polycrystalline materials with heterogeneous particles. to be published in Int. J. Plast.

Bruzzi, M.S., McHugh, P.E., O'Rourke, F., and Linder, T., 2001. Micromechanical modelling of the static and cyclic loading of an Al 2124-SiC MMC. Int. J. Plast. 17, 565-599.

Busso, E.P., Meissonnier, F.T., and O'Dowd, N.P., 2000. Gradient-dependent deformation of two-phase single crystals. J. Mech. Phys. Sol. 48, 2333-2361.

Fedelich, B., 2002. A microstructural model for the monotonic and the cyclic mechanical behavior of single crystals of superalloys at high temperatures. Int. J. Plast. 18, 1-49.

Hart, E.W., 1972. Theory of dispersion hardening in metals. Acta Metall. 20, 275-289.

Hill, R., 1966. Generalized constitutive relations for incremental deformation. J. Mech. Phys. Sol. 14, 95-102.

Hiratani, M., Zbib, H.M., and Khaleel, M.A., 2003. Modeling of thermally activated dislocation glide and plastic flow through local obstacles., Int. J. Plast., 19, 1271-1296.

Hirsch, P. B., 1975. Some aspects of the plastic deformation of dispersion hardened alloys. In: Li, J.C.M., Mukherjee, A.K., (Eds.), Rate processes

in plastic deformation of materials, Proceedings from the John E. Dorn symposium / sponsored by the Flow and Fracture Activity of the Materials Science Division, American Society for Metals, Metals Park, Ohio, p. 1.

Humphreys, F.J., 2000. Particle stimulated nucleation of recrystallization at silica particles in nickel. Scripta Mater. 43, 591-596.

Humphreys, F.J. and Hatherly, M., 1996. Recrystallization and related annealing phenomena, Pergamon, Oxford, 21, 144.

Ishikawa, N., Parks, D.M., Socrate, S. and Kurihara, M., 2000. Micromechanical modeling of Ferrite-Pearlite steels using finite element unit cell models. ISIJ international. 40, 1170-1179.

Khraishi, T.A., and Zbib, H.M., 2002. Dislocation dynamics simulations of the interaction between a short rigid fiber and a glide circular dislocation pile-up. Comp. Mat. Sci. 24, 310-322.

Li, Z. and Guo, W., 2002. The influence of plasticity mismatch on the growth and coalescence of spheroidal voids on the bimaterial interface. Int. J. Plast. 18, 249-279.

Li, Z., Wang, C. and Guo, W., 2003. The evolution of voids in the plasticity strain hardening gradient materials. Int. J. Plast. 19, 213-234.

McHugh, P.E., Asaro, R.J., and Shih, C.F., 1991. Computational modeling of metal matrix composite materials. In: Low, T.C., Rollett, A.D., Follansbee, P.S. and Daehn, G.S., (Eds.), Modeling the deformation of crystalline solids. The Minerals, Metals & Materials Society, p369.

McHugh, P.E., Asaro, R.J., and Shih, C.F., 1993. Computational modeling of metal matrix composite materials-1. Isothermal deformation patterns in

ideal microstructures. Acta metall. mater. 40, 1461-1476.

Nagayama, N., Abe, T. and Nagaki, S., 1986. Plastic deformation of inhomogeneous material with ellipsoidal inclusions. Trans. Japan Society for Mechanical Engineers. A-55, 1365-1373. (written in Japanese)

Ohashi, T., 1987. Computer simulation of non-uniform multiple slip in face centered cubic bicrystals. Trans. Japan Inst. Metals. 28, 906-915.

Ohashi, T., 1994. Numerical modelling of plastic multislip in metal crystals of f.c.c. type. Phil. Mag. A70, 793-803.

Ohashi, T., 1997. Finite-element analysis of plastic slip and evolution of geometrically necessary dislocations in fcc crystals. Phil. Mag. Lett. 75, 51-57.

Ohashi, T., 1999. Evaluation and visualization of geometrically necessary dislocations in metal microstructures by means of continuum mechanics analysis. J. Phys. IV France. 9, Pr9-279-284.

Ohashi, T., and Asakawa, K., 2002. Three dimensional dislocation structure formed in the vicinity of spherical inclusions. Trans. Japan Society for Mechanical Engineers. 68, 1513-1519 . (written in Japanese)

Ohashi, T., 2003. A new model of scale dependent crystal plasticity analysis. submitted to IUTAM symposium on mesoscopic dynamics in fracture process and strength of materials, Osaka, Japan.

Schacht, T., Untermann, N., and Steck, E., 2003. The influence of crystallographic orientation on the deformation behaviour of single crystals containing microvoids., to be published in Int. J. Plast.

Schmitt, C., Lipinski, P., and Berveiller, M., 1997. Micromechanical

modelling of the elastoplastic behavior of polycrystals containing precipitates- application to hypo- and hyper- eutectoid steels., Int. J. Plast., 13, 183-199.

Weertman, J., 2002. Anomalous work hardening, non-redundant screw dislocations in a circular bar deformed in torsion, and non-redundant edge dislocations in a bent foil. Acta Mat. 50, 673-689.

Yamada, Y., Yoshimura, N. and Sakurai, T., 1968. Plastic stress-strain matrix and its application for the solution of elastic-plastic problems by the finite element method. Int. J. Mech. Sci. 10, 343-354.

Zienkiewicz, O.C., 1977. The finite element method, third edition. McGraw-Hill, London, p141.

Postal address of the author.

Tetsuya OHASHI,

Mechanical Systems Department, Kitami Institute of Technology,

Koencho 165, Kitami, Hokkaido, 090-8507, Japan

Figure captions

Figure 1 Matrix-inclusion system employed for the numerical analysis. The microstructure with cuboidal shaped inclusion is also used. The inclusion is embedded at the center of a cuboidal shaped matrix. The diameter of the spherical inclusion and the lateral dimension of the cuboidal one are the same and equal 4 μm, while the lateral dimension of the whole specimen is 30 μm. Normal vector of the primary slip plane and the slip direction lie parallel to the x-y plane.

Figure 2 Crystal orientations of the matrix and the inclusion. The matrix and the inclusion have the same orientations. Slip plane and slip direction of the primary slip system are indicated by open symbols △ and ○, while the ones for the secondary slip system a3 are shown by filled symbols ▲ and ●, respectively.

Figure 3 Length and thickness for the graphical representation of dislocation segments as a function of the dislocation density $\left\|\rho_G^{(n)}\right\|$.

Figure 4 Characteristic angle φ of dislocation segments. We can assign colors for the segments as a function of φ.

Figure 5 (a) Numerical result for the distribution of GN dislocations on the primary slip system in the microstructure with cuboidal shaped inclusion. The average tensile strain for the whole specimen is 0.51%. Dislocations with density smaller than 0.6×10^{11} m^{-2} are omitted from the graphics. (b) Schematic illustration of the three dimensional structure of GN dislocations. W1 and W2 consist of positive and negative edge type dislocations, respectively, and they form dislocation walls growing

perpendicular to the slip plane. L1 indicates loop shaped structures which surround the inclusion.

Figure 6 Structure of GN dislocations on the primary slip system around the spherical shaped inclusion. Only a central part of the whole specimen is shown. The set of parameters d_1=0.25, d_2=5 and d_3=12 x 10^{12} m^{-2} were used for the graphics.

Figure 7 Imaginary foils f1 - f3 in the specimen, which are placed parallel to the primary slip plane and positioned at different distances from the center of the inclusion.

Figure 8 (a), (c) and (e): GN dislocations in the foils f1, f2 and f3, respectively. (b), (d) and (f): schematic illustration for the structure of the GN dislocations in the foils f1, f2 and f3, respectively.

Figure 9 The maximum densities of GN dislocations on twelve slip systems in the microstructure with the spherical inclusion.

Figure 10 Generation of GN dislocations on the a3 slip system.

Figure 11 GN dislocations on the primary (b4) slip system in the microstructures with deformable inclusion of (a) cuboidal and (b) spherical shape.

Figure 12 Distribution of the density norm of GN dislocations $\left\|\rho_G^{(b4)}\right\|$ in the microstructures with deformable inclusion of (a) cuboidal and (b) spherical shape. The average tensile strain in the whole specimen is 0.2%.

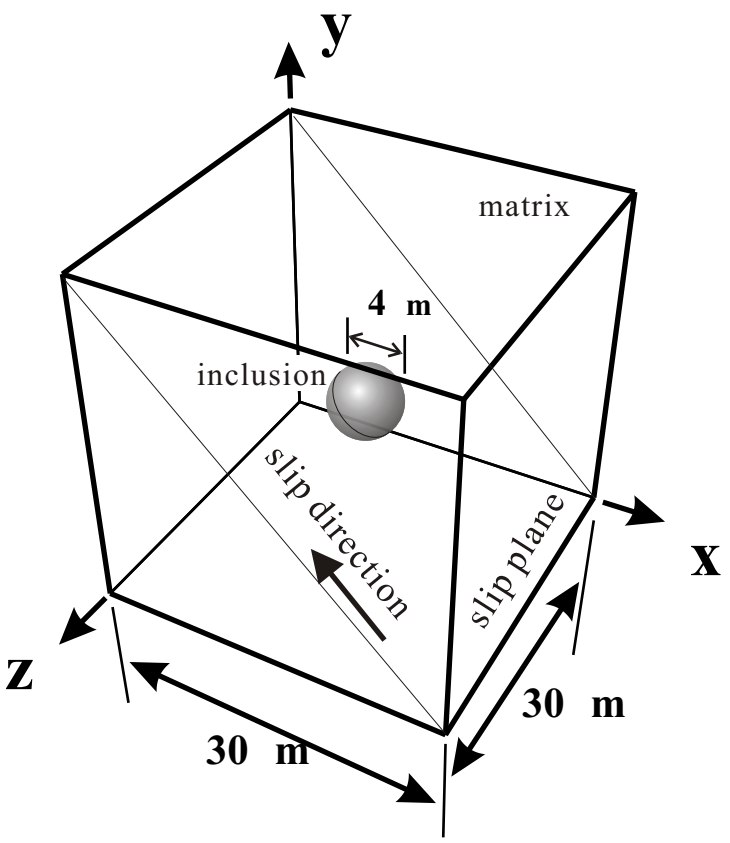

Fig.1

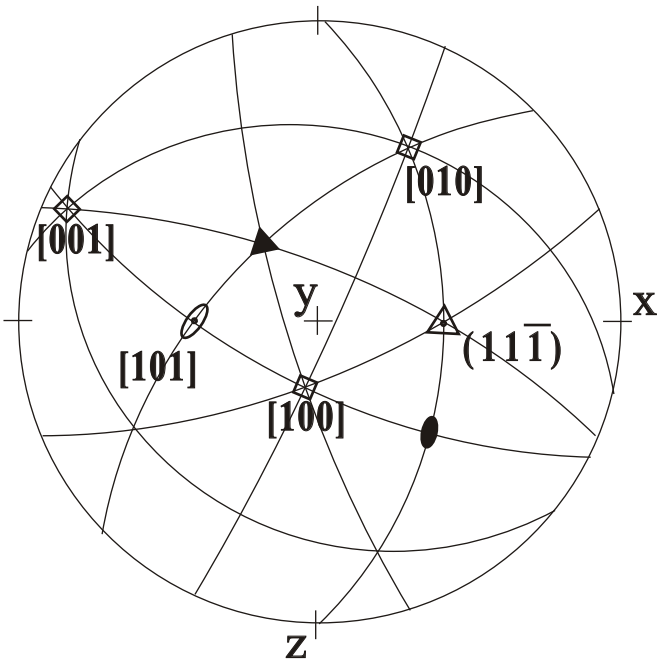

Fig.2

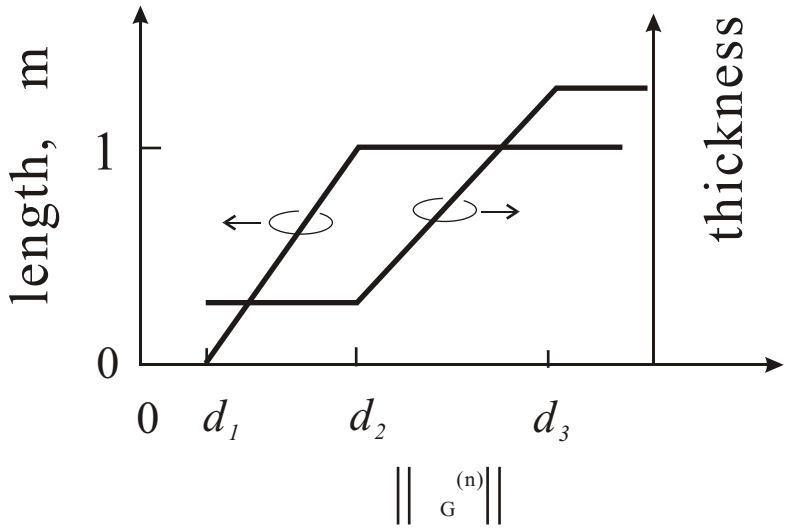

Fig.3

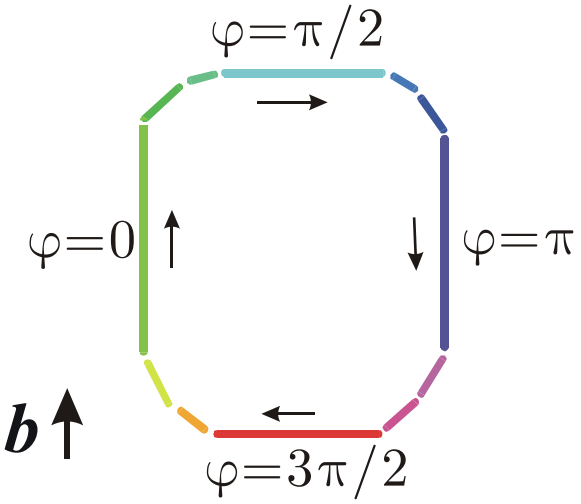

Fig.4

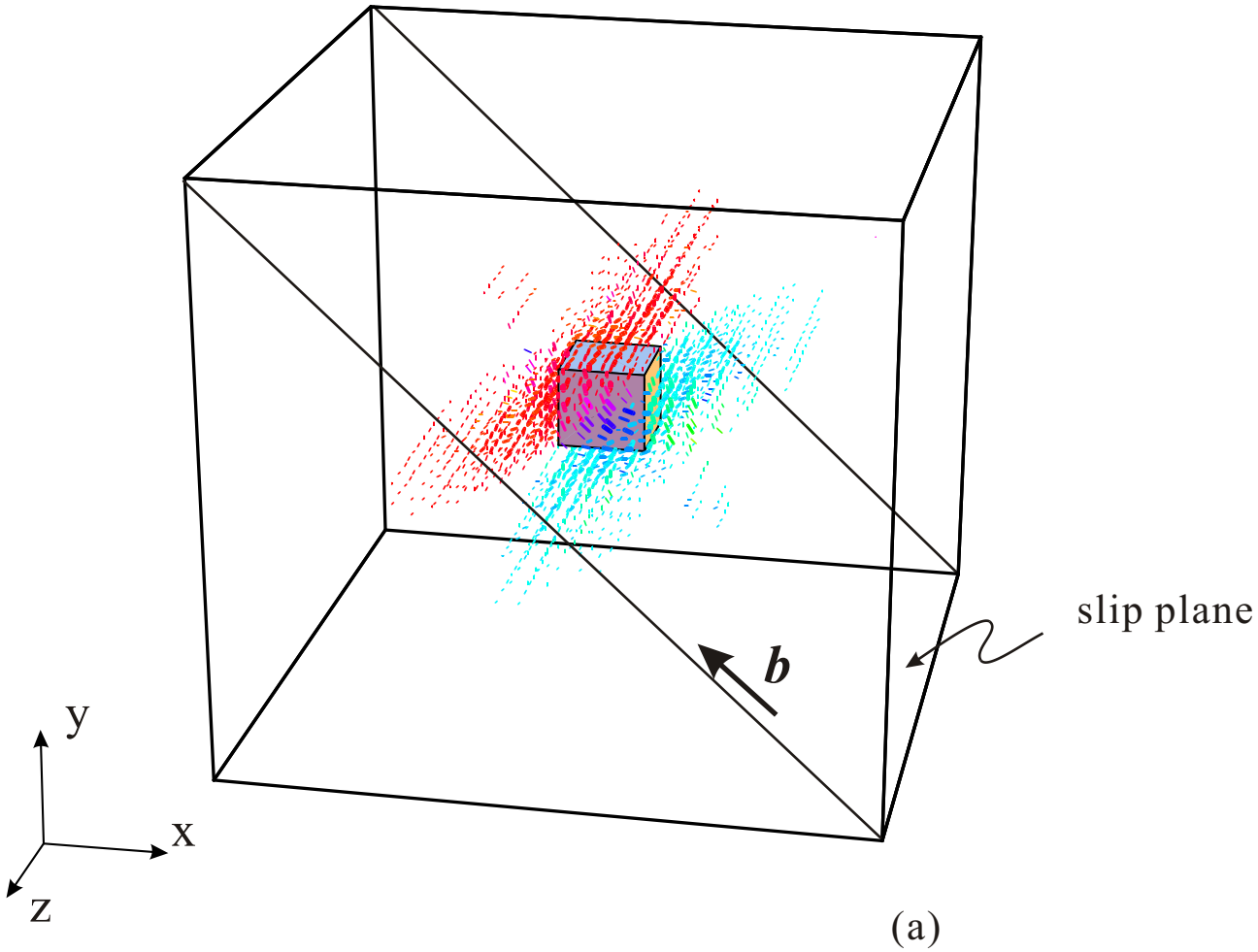
slip plane
b
y
x
z

(a)

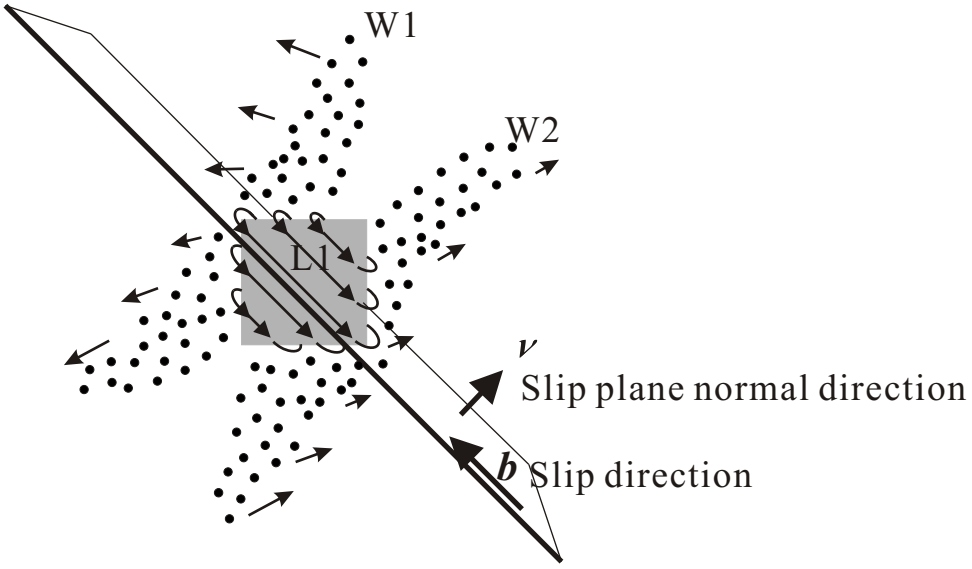
W1
W2
L1
ν
Slip plane normal direction
b
Slip direction

(b)

Fig.5

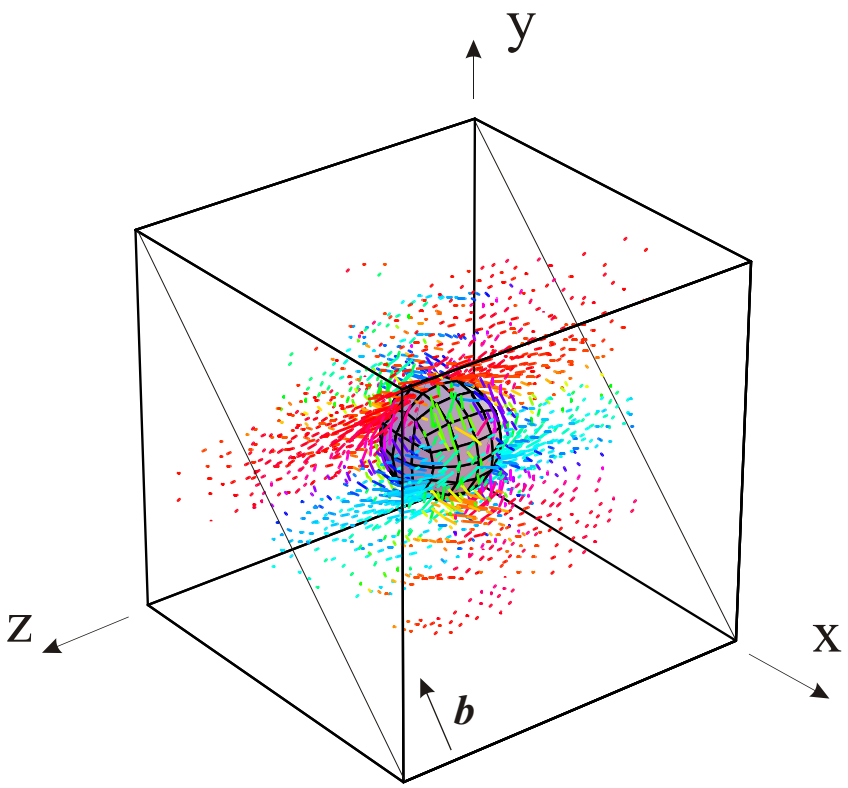

Fig.6

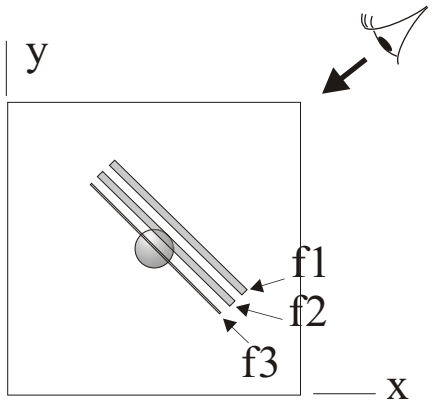

Fig. 7

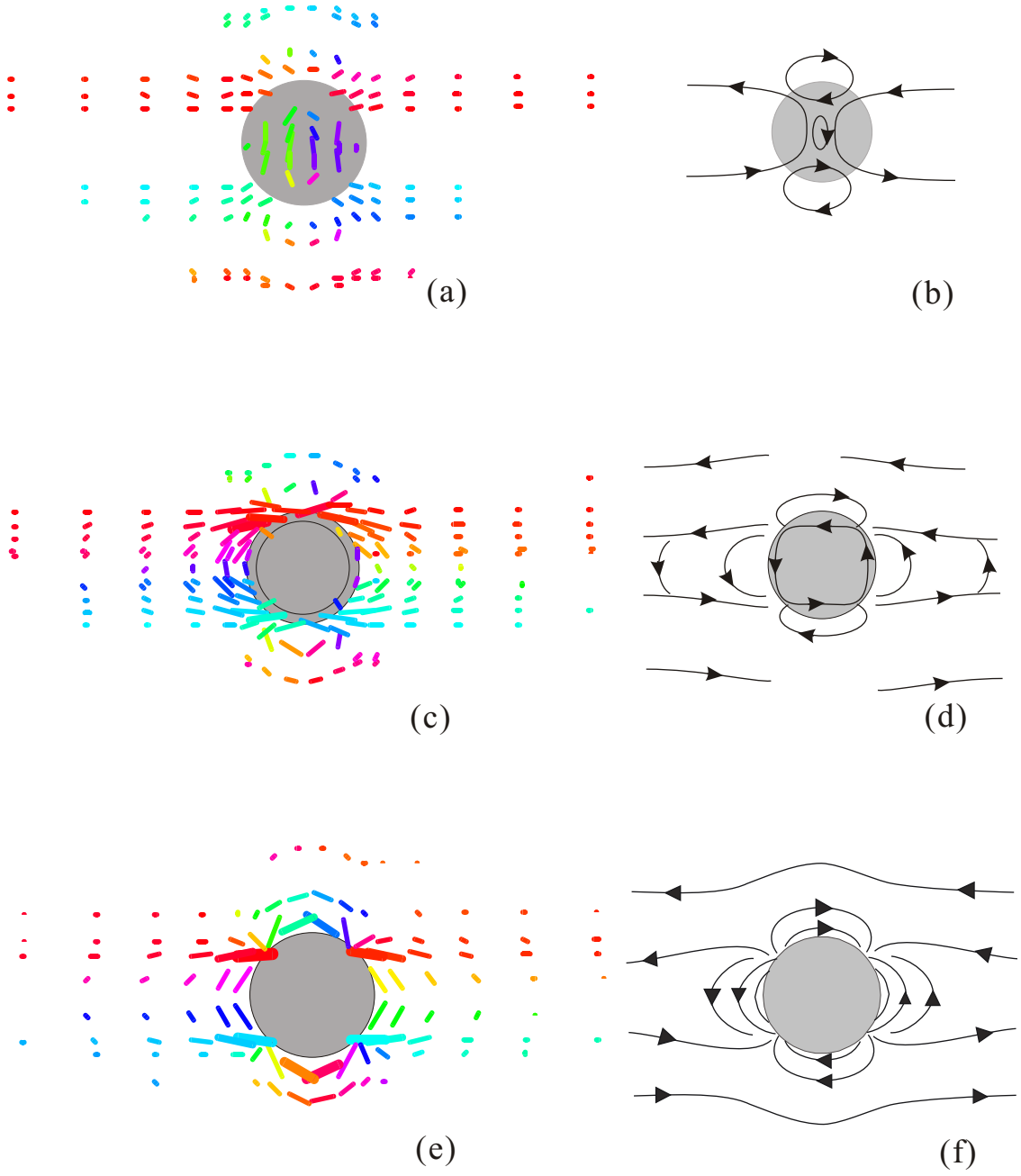

Fig. 8

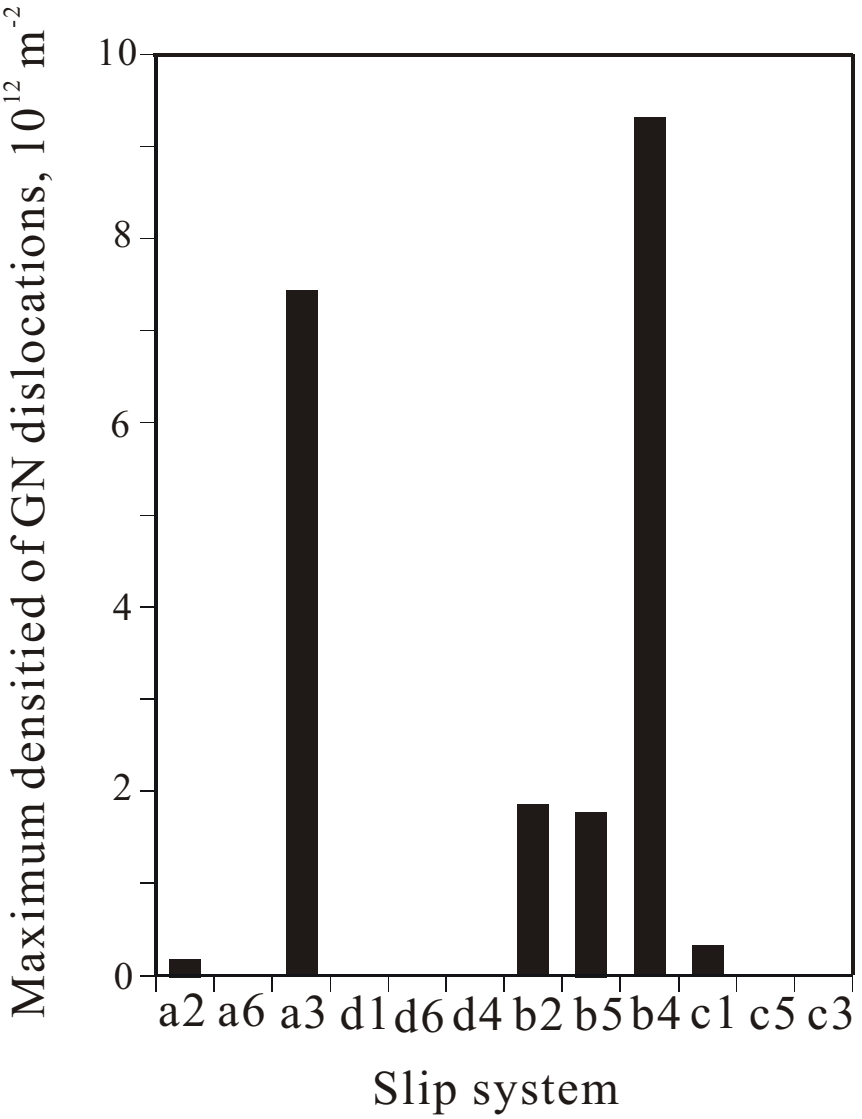
Maximum densitied of GN dislocations, 10^{12} m^{-2}
10
8
6
4
2
0
a2 a6 a3 d1 d6 d4 b2 b5 b4 c1 c5 c3
Slip system

Fig. 9

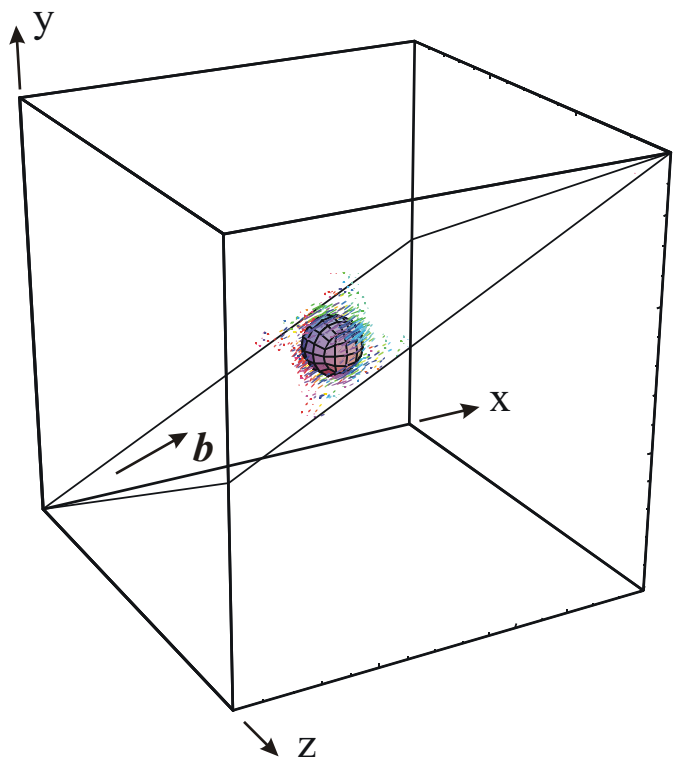

Fig. 10

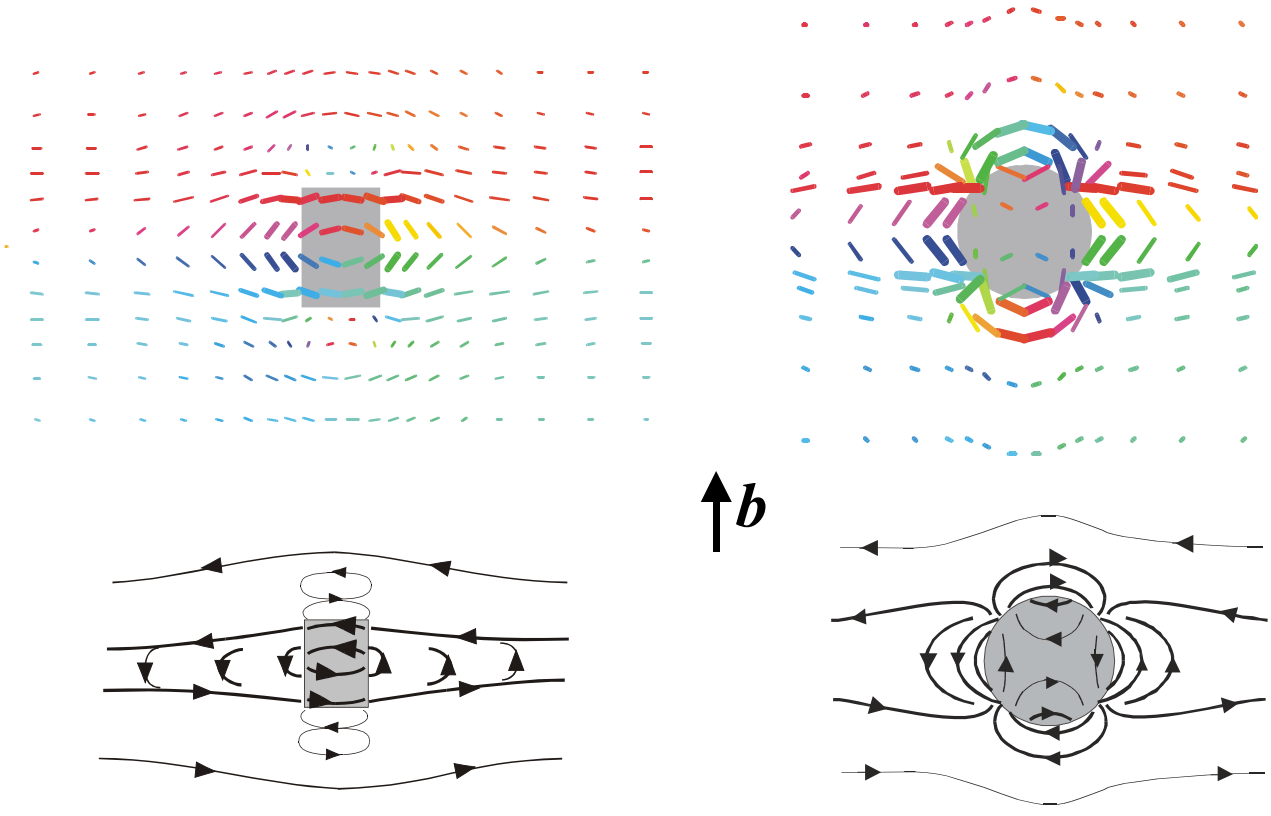

Fig. 11

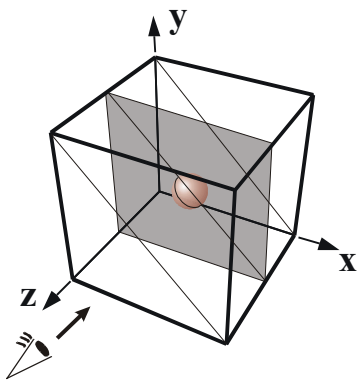
y
x
z

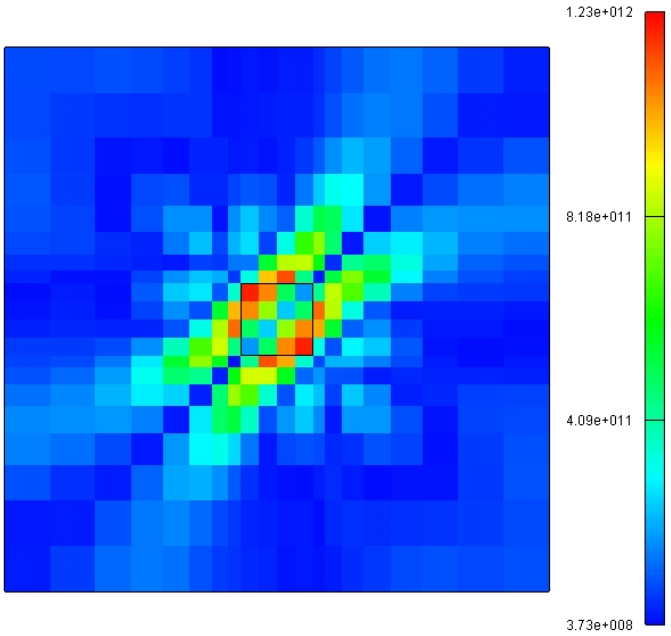
1.23e+012
8.18e+011
4.09e+011
3.73e+008

(a)

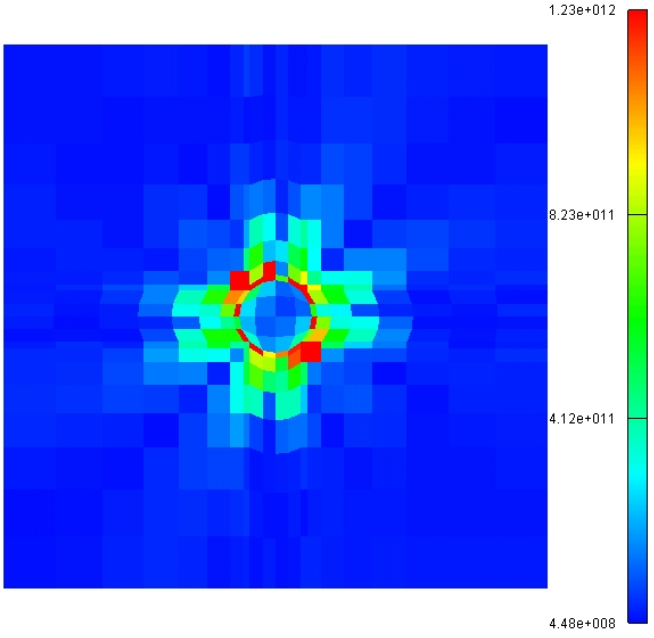
1.23e+012
8.23e+011
4.12e+011
4.48e+008

(b)

Fig. 12

Table 1 Slip systems

Slip systems No.	Schmid-Boas notation	Slip plane	Slip direction
1	a2	$(1\,1\,1)$	$[1\bar{1}0]$
2	a6	↑	$[01\bar{1}]$
3	a3	↑	$[10\bar{1}]$
4	d1	$(\bar{1}\,1\,1)$	$[110]$
5	d6	↑	$[01\bar{1}]$
6	d4	↑	$[101]$
7	b2	$(1\,1\,\bar{1})$	$[1\bar{1}0]$
8	b5	↑	$[011]$
9	b4	↑	$[101]$
10	c1	$(1\,\bar{1}\,1)$	$[110]$
11	c5	↑	$[011]$
12	c3	↑	$[10\bar{1}]$

Table 2 Dislocation interactions and components of the interaction matrix.

Dislocation interaction		(nm)
Elastic interaction	Primary as against primary	1
	Primary as against coplanar	R1
Junction formation	Hirth lock formation	R2
	Glissile jog	R3
	Lomer-Cottrell sessile dislocation	R3'
	Kink formation	R4

Table 3 Stress state in the deformable and non-deformable inclusion with cuboidal shape.

	Deformable inclusion / Non-deformable inclusion			
	Max.	**Min.**	**mean**	(unit:MPa)
xx	-21.4 / -30.0	-28.5 / -62.1	-24.9 / -44.7	
yy	128.6 / 160.4	121.4 / 130.0	125.1 / 144.5	
zz	2.7 / 8.6	-2.8 / 10.0	-0.1 / -0.5	
xy	1.1 / 3.0	-0.7 / -2.4	0.2 / 0.3	
yz	1.9 / 2.5	-1.6 / -2.3	0.2 / 0.1	
zx	1.9 / 2.1	-1.7 / -2.9	0.1 / -0.2	